Ocean Dynamics (2005)
DOI 10.1007/s10236-005-0008-3

W. P. Budgell

Numerical simulation of ice-ocean variability in the Barents Sea region

Towards dynamical downscaling

Received: 4 January 2005 / Accepted: 6 June 2005
© Springer-Verlag 2005

Abstract A dynamic–thermodynamic sea ice model has been coupled to a three-dimensional ocean general circulation model for the purpose of conducting ocean climate dynamical downscaling experiments for the Barents Sea region. To assess model performance and suitability for such an application, the coupled model has been used to conduct a hindcast for the period 1990–2002. A comparison with available observations shows that the model successfully tracks seasonal and inter-annual variability in the ocean temperature field and that the simulated horizontal and vertical distribution of temperature are in good agreement with observations. The model results follow the seasonal and inter-annual variability in sea ice cover in the region, with the exception that the model results show too much ice melting in the northern Barents Sea during summer. The spatial distribution of the winter simulated sea ice cover is in close agreement with observations. Modelled temperatures and ice concentrations in the central Barents Sea are biased too high and too low, respectively. The probable cause is too high inflow of Atlantic Water into the Barents. The seasonal and inter-annual fluctuations in temperature and sea ice cover in the central Barents are, however, in excellent agreement with observations. Salt release during the freezing process in the numerical simulation exhibits considerable inter-annual variability and tends to vary in an opposite manner to the net inflow volume flux at the western entrance of the Barents Sea. Overall, the model produces realistic ice-ocean seasonal and inter-annual variability and should prove to be a useful tool for dynamical downscaling applications.

Responsible Editor: Phil Dyke

W. P. Budgell (✉)
Institute of Marine Research and Bjerknes Centre for Climate Research, Postbox 1870, Nordnes, 5817 Bergen, Norway
E-mail: paul.budgell@imr.no

Keywords Ice-ocean model · Comparison model-data · Barents Sea

1 Introduction

A regional coupled ice-ocean model will be used to study future climate change scenarios in the Barents Sea based on results from the global Bergen Climate Model (Furevik et al. 2003). However, before future regional climate regimes can be simulated, it is necessary to demonstrate that the downscaling model can reproduce current climate conditions with realistic seasonal and inter-annual variability, which is the main goal of this paper.

The Barents Sea (Figs. 1, 2), linking the Nordic Seas with the Arctic Ocean, is an important fisheries region (Sakshaug et al. 1994). The climate variability of the Barents Sea has a strong influence on reproduction, recruitment (Sætersdal and Loeng 1987; Ellertsen et al. 1989), growth and distribution (Nakken and Raknes 1987; Michalsen et al. 1998) of fish species in the region. To address the implications of future climate change on the Barents Sea region, an ocean climate dynamical downscaling exercise has been initiated as part of the Research Council of Norway's RegClim (Regional Climate development under global warming) programme. Dynamical downscaling is the production of high temporal and spatial resolution climate forecasts using regional models to 'downscale' coarsely resolved global climate model results.

Section 2 provides a description of the coupled ice-ocean model together with the configuration of the large-area (basin-scale) and nested (regional-scale) models. The boundary and initial conditions are defined and the surface forcing fields used in the models are discussed. Section 3 contains the results of the validation of the regional model against observations. Comparisons of model results with satellite imagery, hydro-

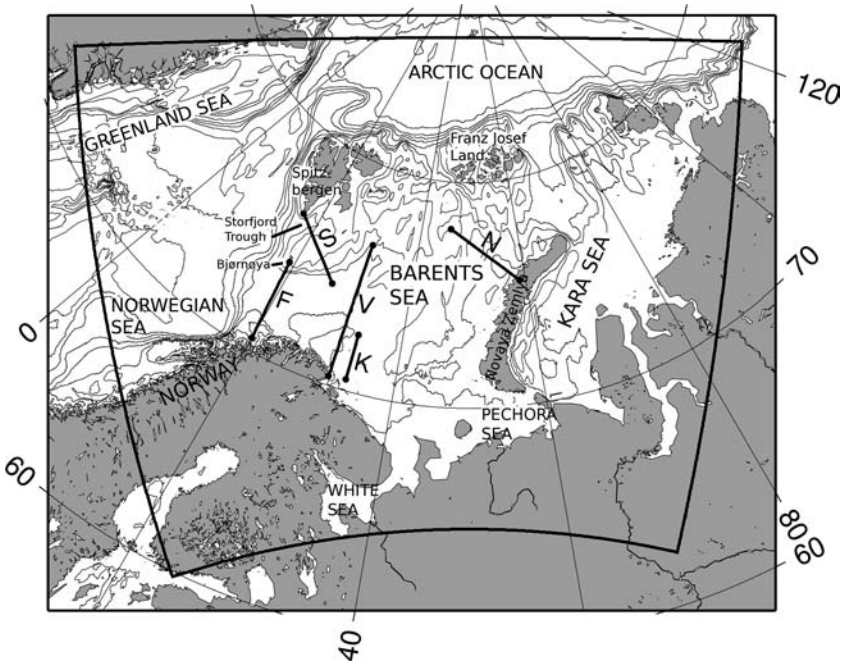

Fig. 1 Barents Sea regional model domain showing the location of sections: *F* (Fugløya-Bjørnøya), *K* (Kola), *V* (Vardø North), *S* (Spitzbergen Bank) and *N* (West Novaya Zemlya)

Fig. 2 Large-area model domain showing the location of the nested Barents Sea regional model domain

graphic sections and spatially integrated time series are provided. Section 4 offers examples of the results of ice–ocean interaction in the Barents Sea. Brine formation and meltwater production are illustrated and discussed. Finally, the paper concludes in Sect. 5 with a summary and discussion of results.

2 The ice-ocean model

Several model studies of circulation in the Barents Sea region have been carried out over the past decade or so, including those of (Ådlandsvik and Loeng 1991; Stolehansen and Slagstad 1991; Harms 1992; Loeng et al. 1997; Harms 1997; Ådlandsvik and Hansen 1998; Asplin et al. 1998; Ingvaldsen et al. 2004a; Maslowski et al. 2004). The current study is based on a new ice-ocean model system run at high spatial resolution for a multiyear simulation validated against available observations.

2.1 The ocean model component

The ocean model component is based on Regional Ocean Modelling System (ROMS) version 2.1. ROMS is a three-dimensional baroclinic general ocean model, the development of which is described in a series of papers (Song and Haidvogel 1994; Haidvogel and Beckmann 1999; Haidvogel et al. 2000; Shchepetkin and McWilliams 2003). ROMS uses a topography-following coordinate system in the vertical that permits enhanced resolution near the surface and bottom (Song and Haidvogel 1994). Orthogonal curvilinear coordinates are used in the horizontal. A spline expansion can be used for vertical discretization which provides for an improved representation of the baroclinic pressure gradient (Shchepetkin and McWilliams 2003), vertical advection and vertical diffusion of momentum and tracers. ROMS has been designed from the ground up to run efficiently in both distributed (MPI) and shared (OpenMP) memory parallel computing environments, thus enabling computationally intensive dynamical downscaling experiments to be conducted.

2.2 The ice model component

Large portions of the Barents Sea are ice-covered for much of the year. Thus, it is important to include the effects of ice drift, melting and freezing upon the ocean fields. To accomplish this, a dynamic–thermodynamic sea ice module has been developed and coupled to the ocean model. The ice dynamics are based upon an elastic-viscous-plastic (EVP) rheology after Hunke and Dukowicz (1997) and Hunke (2001). The EVP scheme is based on a time-splitting approach whereby short elastic time steps are used to regularize the solution when the ice exhibits nearly rigid behaviour. Because the time discretization uses explicit time-stepping, the ice dynamics are readily parallelizable and thus computationally efficient. Employing linearization of viscosities about ice velocities at every elastic (short) time step, as recommended by Hunke (2001), has the desirable property of maintaining the ice internal stress state on or in the plastic yield curve. That is, the ice deforms as a plastic material unless it is in a rigid state. Another desirable property of the Hunke (2001) linearization is that the EVP ice dynamics are found to provide a good transient response to rapidly varying winds as well as to inertial and tidal dynamics, particularly in the marginal ice zone.

The ice thermodynamics are based on those of Mellor and Kantha (1989) and Häkkinen and Mellor (1992). Two ice layers and a single snow layer are used in solving the heat conduction equation. The snow layer possesses no heat content, but is, in effect, an insulating layer. Surface melt ponds are included in the ice thermodynamics. A molecular sub-layer (Mellor et al. 1989) separates the bottom of the ice cover from the upper ocean. The inclusion of the molecular sub-layer was found to produce much more realistic freezing and melting rates than if the ice-ocean heat flux is based purely on the ice bottom–ocean upper layer temperature difference.

2.2.1 The large-area model

The large-area model (Fig. 2) is used to supply boundary and initial conditions to the regional Barents model. A stretched spherical coordinate grid (Bentsen et al. 1999) is used in the horizontal, with the North Pole situated in central Asia and the South Pole situated in the Pacific Ocean west of North America. In the Barents Sea region, the horizontal resolution is approximately 50 km. There were 30 generalized σ-coordinate (s) levels, stretched to increase vertical resolution near the surface and bottom.

A time step of 1,800 s was used for both the ocean internal mode and ice thermodynamic time step. A ratio of 40 was used between the ocean internal and external mode time steps. A ratio of 60 was used between ice thermodynamic and dynamic time steps.

No tides were included in the simulation. The vertical mixing scheme employed was the LMD (Large et al. 1994) parameterization. The LMD scheme was used for the large-area model because it has been found to produce good agreement with observed mixed-layer behaviour in the deep ocean (Large and Gent 1999). The lateral boundaries were closed with the exception that a constant volume flux of 1 Sv was input across Bering Strait and the same quantity was removed along the southern boundary.

The atmospheric forcing was obtained from the NCEP/NCAR reanalysis data (Kalnay et al. 1996). Daily mean wind stress, and latent, sensible, downward shortwave radiative and net longwave radiative heat fluxes were applied as surface forcing after correcting for differences in model and NCEP surface conditions, such as in surface temperature and ice concentration. The flux corrections applied were developed by Bentsen and Drange (2000) and provide a feedback between the model surface temperature and applied heat fluxes, thus minimizing problems with drift in model surface temperatures. Precipitation was taken from the daily mean NCEP values. Snowfall was taken to be precipitation,

corrected for snow density, when air temperature was less than 0°C. Evaporation was computed from the latent heat flux.

River runoff was computed using the NCEP/NCAR Reanalysis daily accumulated surface runoff values over land that were routed to ocean discharge points using the Total Runoff Integrated Pathways (TRIP) approach of Oki and Sud (1998). The hydrographs were modified for areas north of 60°N to account for permafrost hydrology and storage in snow cover.

The model was started from rest at January 1, 1948 with the January mean temperature and salinity from the Polar Hydrographic Climatology (Steele et al. 2001). Initial sea ice concentration was obtained from the daily mean NCEP/NCAR Reanalysis sea ice concentration for January 1, 1948. Initial average ice thickness (ice volume per unit area averaged over each grid cell) was specified by multiplying the initial ice concentration by 2 m.

A simulation was then conducted to spin up the model over the period 1948 to the end of 1987. The model fields at 0000Z January 1, 1988 were then used as initial conditions for a hindcast conducted from January 1, 1948 to the end of 2003.

Typical results from the large-area model for sea surface temperature (SST) and ice concentration at January 3, 1994 are shown in Figs. 3 and 4, respectively.

From the map of sea surface height from the large-area model on the same date shown in Fig. 5, it can be seen that even though the model resolution in the Gulf Stream region in the western Atlantic is coarse at ~80 km, the Gulf Stream separates from the western boundary at the correct location—Cape Hatteras, 35°N. The basin-scale circulation and temperature patterns are realistic and are suitable for use in boundary forcing of the regional model.

2.3 The Barents regional model

The regional model domain is shown in Fig. 1. The regional model uses the same horizontal coordinate system as the large-area model, but at higher spatial resolution. The horizontal grid size varies between 7.8 and 10.5 km, with an average of 9.3 km. In the vertical, 32 *s*-coordinate levels are used, with enhanced resolution near the surface and bottom.

The generic length scale (GLS) scheme (Warner et al. 2005) was used for subgrid-scale mixing of mass and momentum, with the two-equation *k-kl* model parameters. The *k-kl* model is a modified form of the Mellor-Yamada 2.5 closure (Mellor and Yamada 1982). The GLS *k-kl* scheme was selected for use in the Barents regional model since it was found to produce good results in coastal applications where tidal mixing is important (Warner and Geyer 2005).

The time step used in the simulation was 450 s for both the ocean internal mode and the ice thermodynamics. The ocean model is split mode explicit. The ratio of ocean internal to external mode time step is 45. The ratio of ice thermodynamic to dynamic time step is 60.

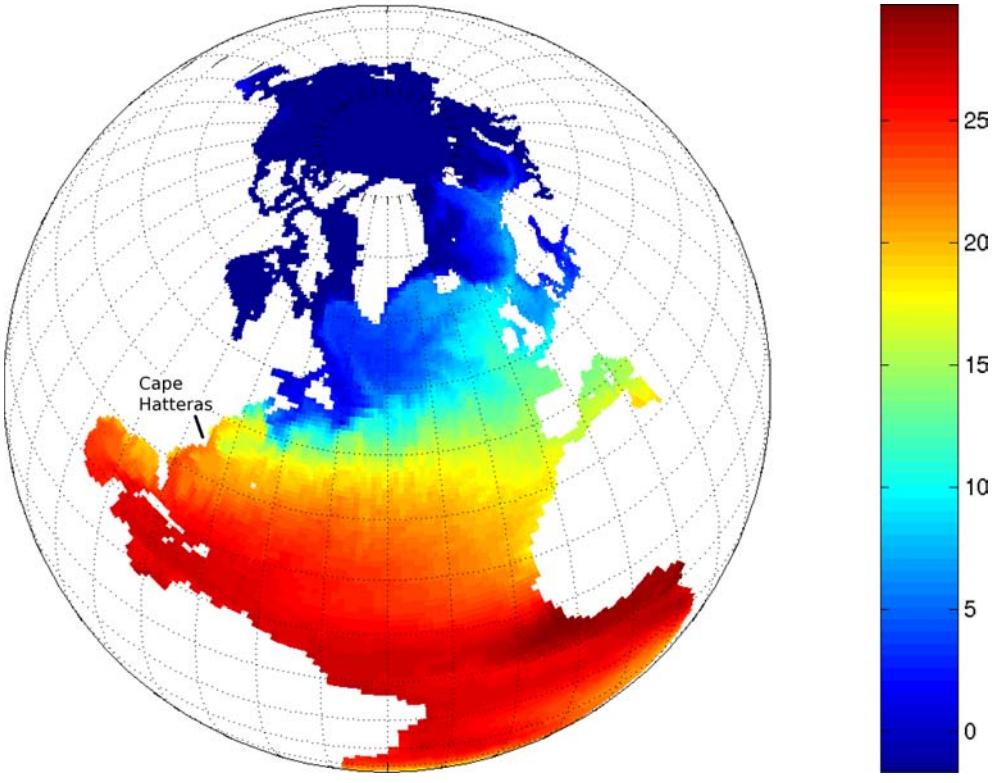

Fig. 3 Typical SST field (°C) from the large-area model, from January 3, 1994

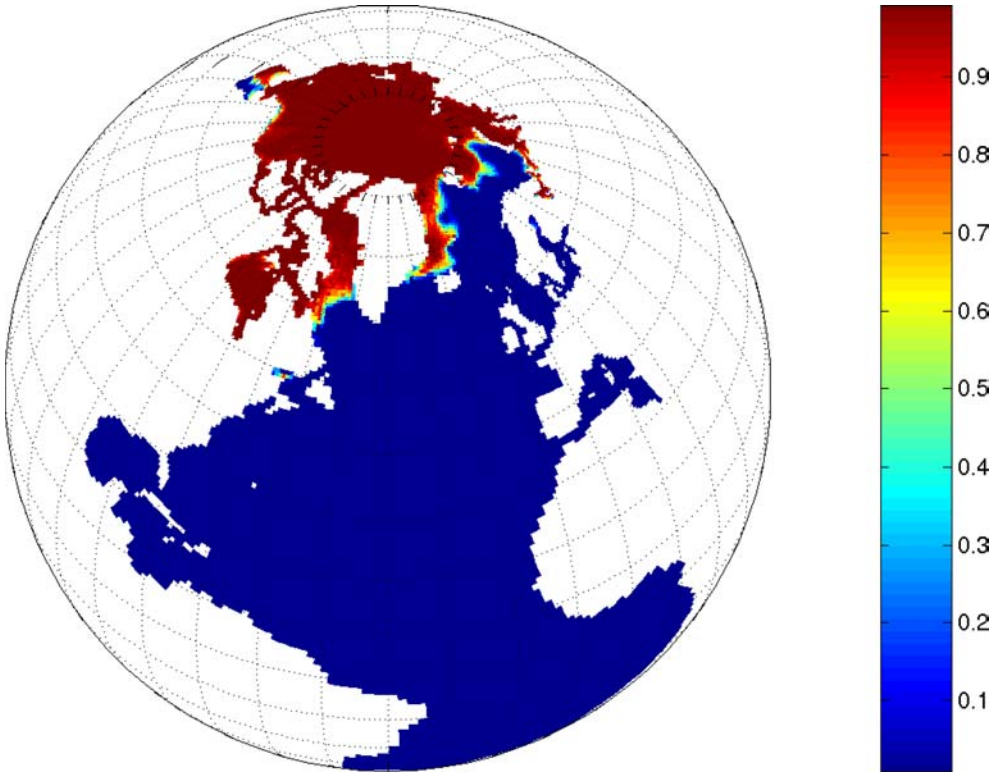

Fig. 4 Typical ice concentration field from the large-area model, from January 3, 1994

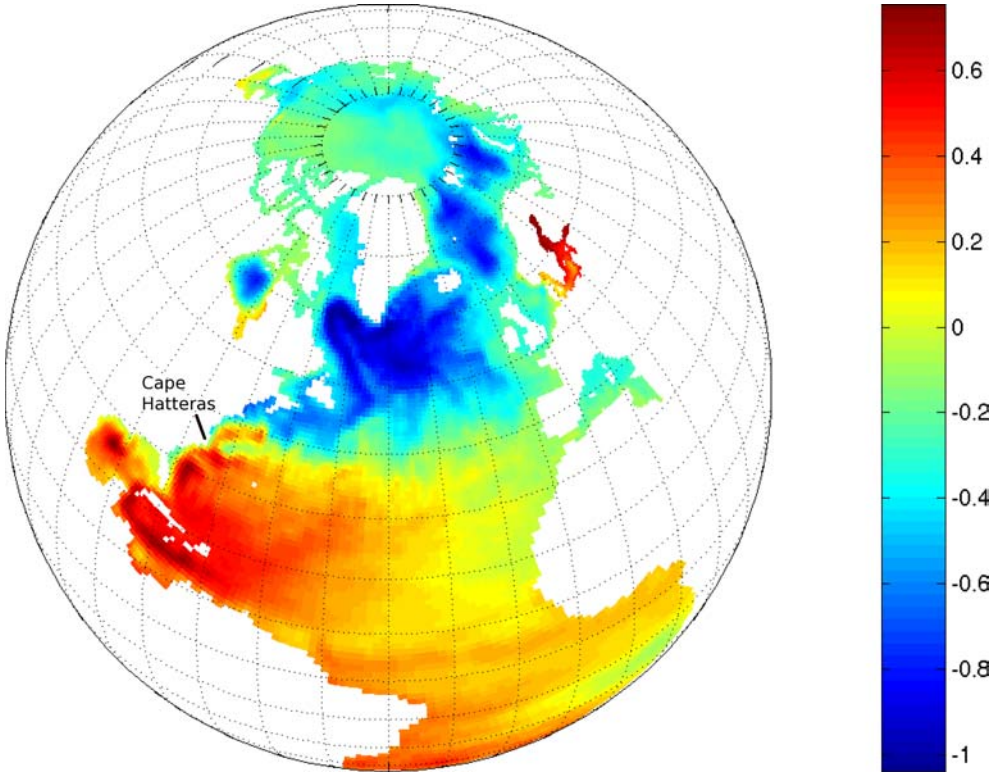

Fig. 5 Typical sea surface height field (m) from the large-area model, from January 3, 1994

Flather (1976) and Chapman (1985) radiation open boundary conditions were prescribed for barotropic normal velocity components and the free surface, respectively. Flow relaxation scheme (Engedahl 1995) open boundary conditions were employed for three-dimensional velocity components and tracers. The regional model was forced at the boundaries with interpolated 5-day mean fields from the large-area model and

with tidal velocities and free surface heights from eight constituents of the Arctic Ocean Tidal Inverse Model (AOTIM) by Padman and Erofeeva (2004).

Surface forcing for the regional model was the same as that applied in the large-area model simulation, but with the exception that the NCEP/NCAR Reanalysis cloud cover fraction was modified to provide the same monthly mean cloud cover climatology over the period 1983–2002 as the International Satellite Cloud Climatology Project (ISCCP) cloud cover data (Schiffer and Rossow 1985). This necessitated the modification of the downward shortwave radiation and net longwave radiation fluxes to be consistent with the new cloud data. In the first simulations of Barents Sea ice cover, we found excessive melting of sea ice in summer by shortwave radiation due to the NCEP/NCAR Reanalysis cloud cover fraction being too low by a factor of approximately 0.75. This problem was largely, but not entirely, remedied by the use of ISCCP cloud cover data.

Initial conditions for the Barents regional model were obtained from the archived 5-day mean large-area model fields interpolated to January 1, 1990. The Barents simulation was conducted for the period 1990–2002.

3 Model-data comparison

Model results are compared with data from a variety of sources, including satellite SST and passive microwave, hydrographic sections and time series of integral quantities.

3.1 Satellite SST

An indication of the spatial structure of the SST can be obtained from SST derived from satellite Advanced Very High Resolution Radiometer (AVHRR) by the Pathfinder programme at the NASA Physical Oceanography Distributed Active Archive Center (PODAAC). Monthly mean, 4-km resolution, best fields from ascending (day-time) orbits are compared with the corresponding model values for March and September, 1993 in Fig. 6. The PODAAC SST fields are interpolated on to the model grid using nearest neighbour interpolation.

It can be seen that, in March, the model produces a realistic transport of warm water northward west of Spitzbergen in the West Spitzbergen Current and that the region encompassed by the 2° isotherm matches the satellite SST distribution, but the model results are ~2° too cold in the middle of the Norwegian Sea near the left-hand (southern) boundary. The model results for September show good agreement with the satellite SST field.

3.1.1 Hydrographic sections

Model results were compared with the Fugløya-Bjørnøya hydrographic section (section F, in Fig. 1). Shown in Fig. 7 are observed and modelled-observed temperatures from August/September in the years 1992–1994. The model-data agreement in these sections are found to be consistent with sections from other times of the year,

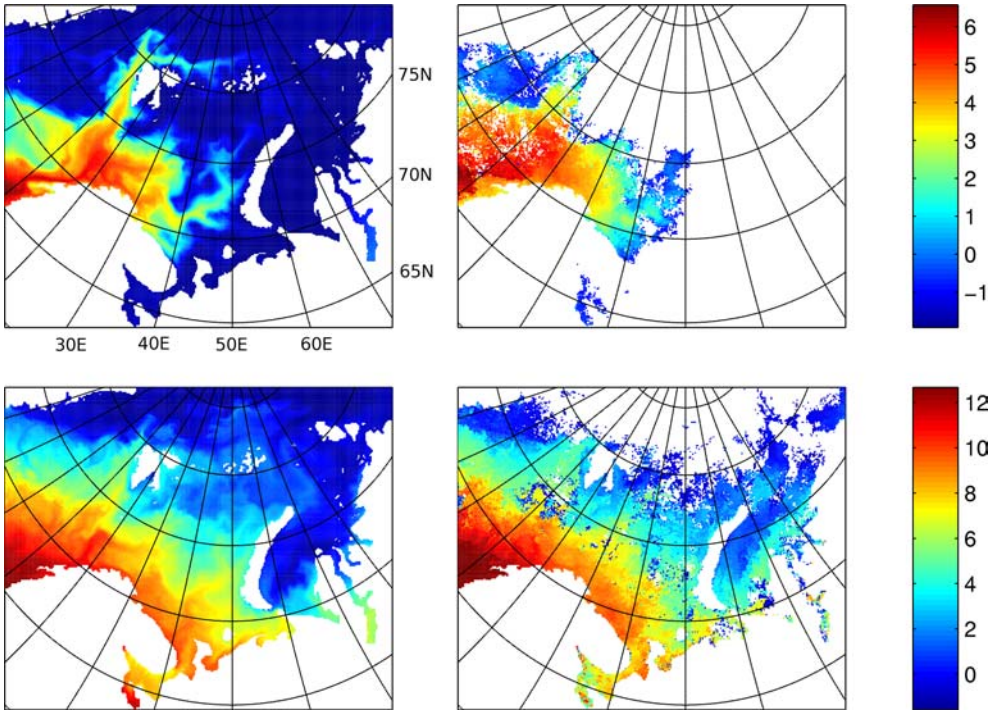

Fig. 6 Modelled versus Pathfinder AVHRR monthly mean SST (°C). The *top row* is from March, 1993, the *lower row* is from September, 1993. The *left-hand column* contains the model fields, the *right-hand panel* contains the Pathfinder AVHRR fields. The modelled and observed fields are in good general agreement. The modelled March SST field is not diffuse enough in the Norwegian Sea (near 68°N, 12°E)

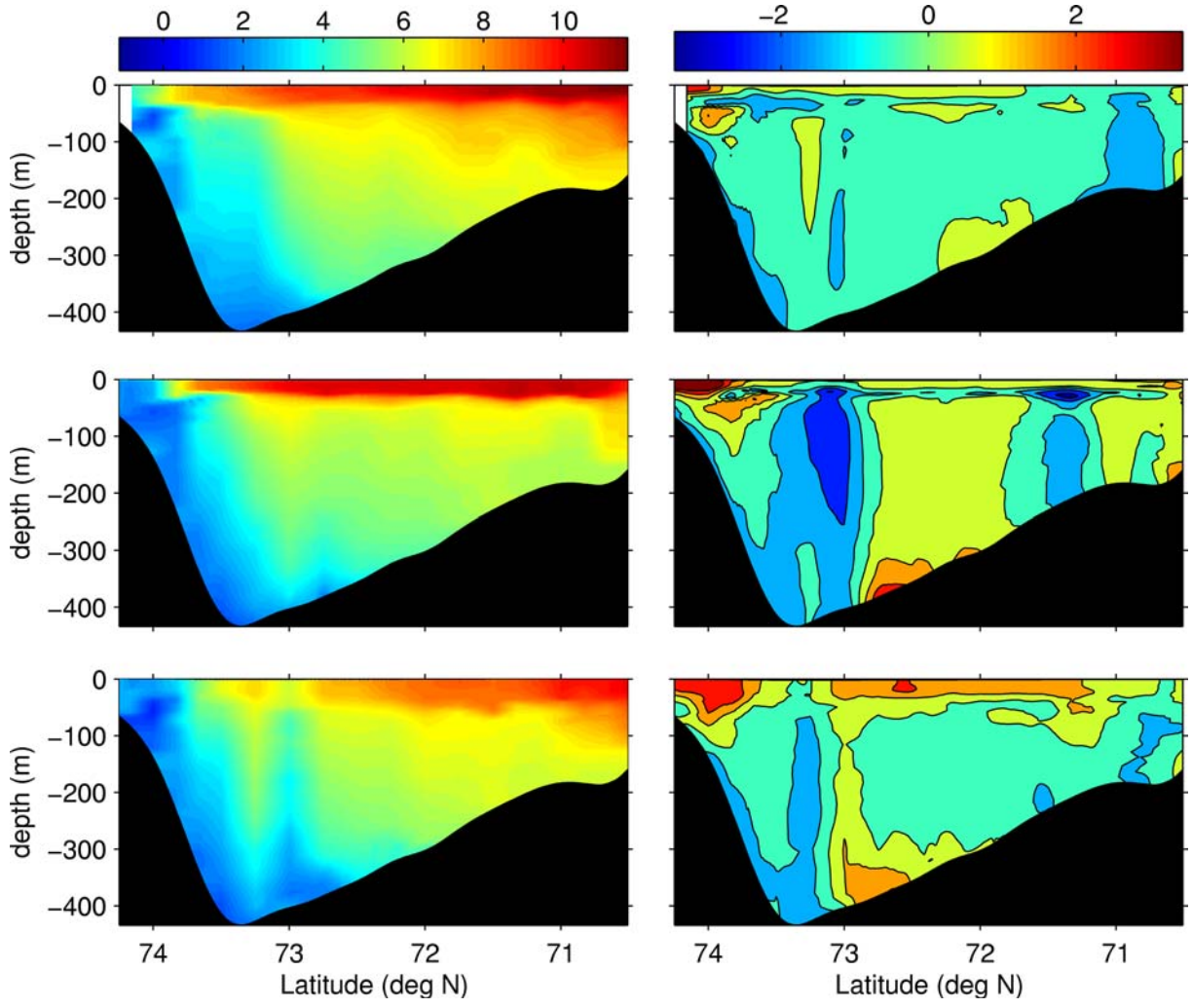

Fig. 7 Observed and modelled-observed temperature (°C) from the Fugløya-Bjørnøya section for August/September, 1992–1994. The *top row* is from 1992, the *middle row* is from 1993 and the *bottom row* is from 1994. The *left-hand column* contains the temperatures from CTD (conductivity–temperature–depth) profiles, the *right-hand column* contains modelled-observed temperatures. Modelled temperatures are daily mean values taken for the day in the middle of the transect (September 3, 1992, August 26, 1993 and September 5, 1994). In the modelled-observed temperature panels, the contour interval is 1°C. The turquoise filled contour interval contains values between −0.5 and 0.5°C. No consistent error pattern is evident across the 3 years, with the exception that the model surface temperatures are too warm near Bjørnøya at the northern end of the section

as well as with the Vardø North sections from various times of the year.

Given that the modelled fields are only averaged over a day and are compared to a (∼2 day) nearly synoptic hydrographic section, the agreement is remarkably good. The model results show good placement of the Polar Front along the Bjørnøya (northern) slope. The GLS mixing scheme produces mixed layers of the right thickness during the stratified late summer conditions. The modelled surface temperatures are too warm in the immediate vicinity of Bjørnøya at the northern end of the section.

Salinity is a much more difficult property to represent correctly, as can be seen from Fig. 8. The modelled Atlantic Water inflow, situated roughly at 71.5–72.5°N, is ∼0.05–0.1 too low. The modelled coastal current at the southern end of the section is too narrow, and is 0.5 too saline. The fresher, colder Arctic Surface Water outflow jet along the slope south of Bjørnøya at the northern end of the section is missing completely in the model results. The lower-salinity Norwegian Coastal Current along the southern portion of the section is too saline in the model results.

3.1.2 Section mean time series

Temperatures have been averaged across portions of three sections in the Barents Sea: Fugløya-Bjørnøya, Vardø North and Kola, sections F, V and K, respectively, in Fig. 1. The Institute of Marine Research in Bergen, Norway, has been monitoring the Fugløya-Bjørnøya section six times per year and the Vardø North section for four times per year for 28 years. Section mean temperatures have been computed over the depth

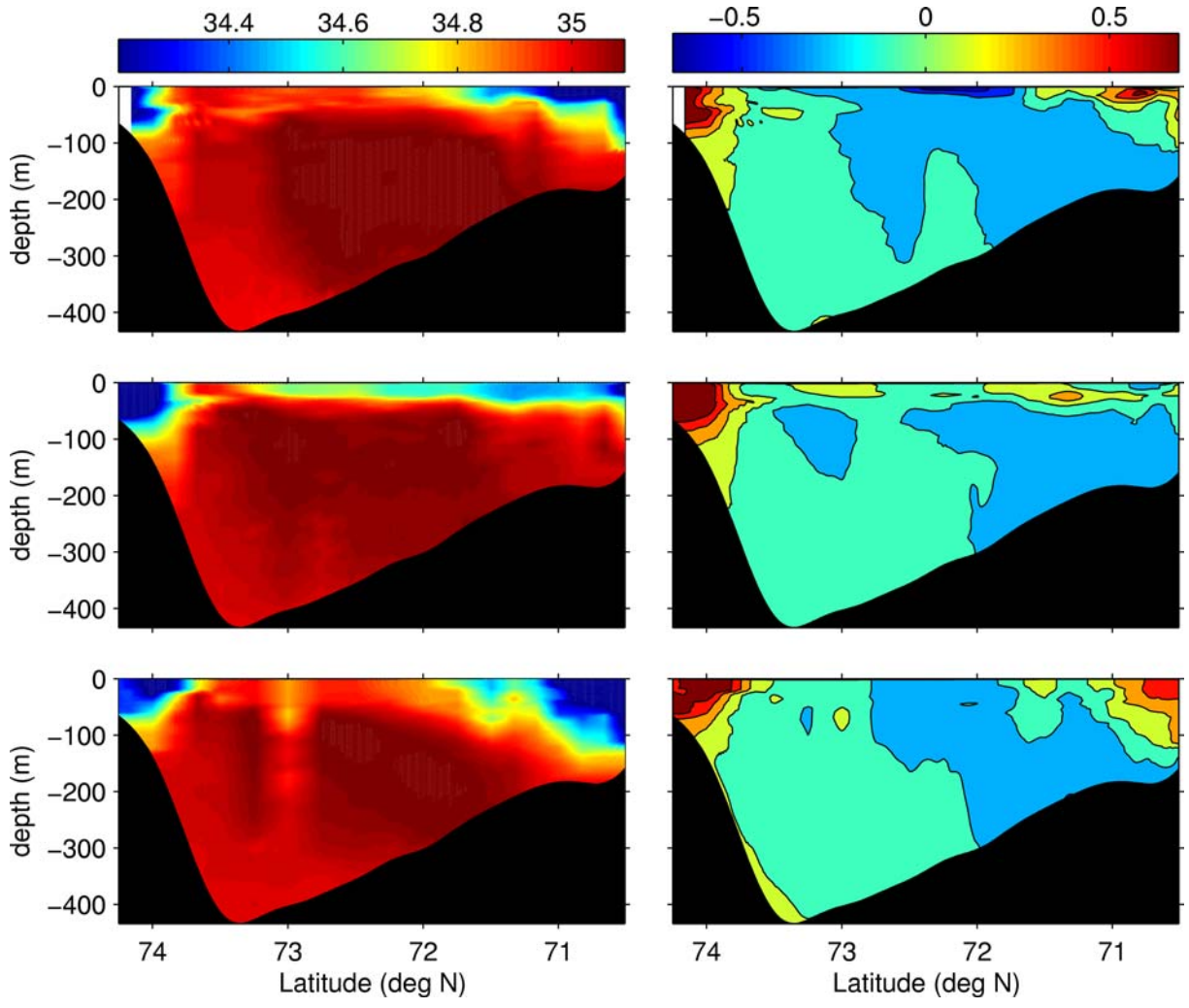

Fig. 8 Observed and modelled-observed salinity from the Fugløya-Bjørnøya section for August/September, 1992–1994. The *top row* is from 1992, the *middle row* is from 1993 and the *bottom row* is from 1994. The *left-hand column* contains the salinity from CTD (conductivity–temperature–depth) profiles, the *right-hand column* contains modelled-observed salinity. Modelled salinities are daily mean values taken for the day in the middle of the transect (September 3, 1992, August 26, 1993 and September 5, 1994). In the modelled-observed salinity panels, the contour interval is 0.2. The turquoise filled contour interval contains values between −0.1 and 0.1. The salinity of the Atlantic Water inflow is roughly 0.05–0.1 too low in the model results. The low salinity cores at the surface near the northern and southern ends of the section are not captured by the model

range of 50–200 m and between 71.5 to 73.5°N from the Fugløya-Bjørnøya section and between 72.25 to 74.25°N from the Vardø North section. Shown in Figs. 9 and 10 are monthly mean-modelled temperatures and averaged temperatures from the Fugløya-Bjørnøya and Vardø North hydrographic sections, respectively. A constant value of 0.5°C was subtracted from the modelled Vardø North temperatures to remove the bias of +0.48°C and simplify the comparison with the observations. The results from both sections show the model is in generally good agreement with the observed seasonal and inter-annual fluctuations.

Temperatures at the Kola section have been monitored back to 1900 (V. Ozhigin, personal communication). The Kola section temperatures have been averaged over the upper 200 m and along the section between 70.5 and 72.5°N at 33.5°E. The Kola section temperature time series has been shown to be related to cod stock recruitment and is a useful indicator of climatic variability in the Barents Sea (Dippner and Ottersen 2001). Thus, the Kola section temperature series is a good validation data set for comparison with model results. Shown in Fig. 11 is a comparison of modelled and observed values of monthly mean Kola section temperatures for the period 1990–2002. A constant value of 0.6°C has been subtracted from the displayed model temperatures to account for the bias of +0.63° in the model results relative to the observations over the period 1991–2002 (ignoring the first year as spin-up).

It can be seen that the model results track the seasonal and inter-annual variations in the Kola section temperatures very well.

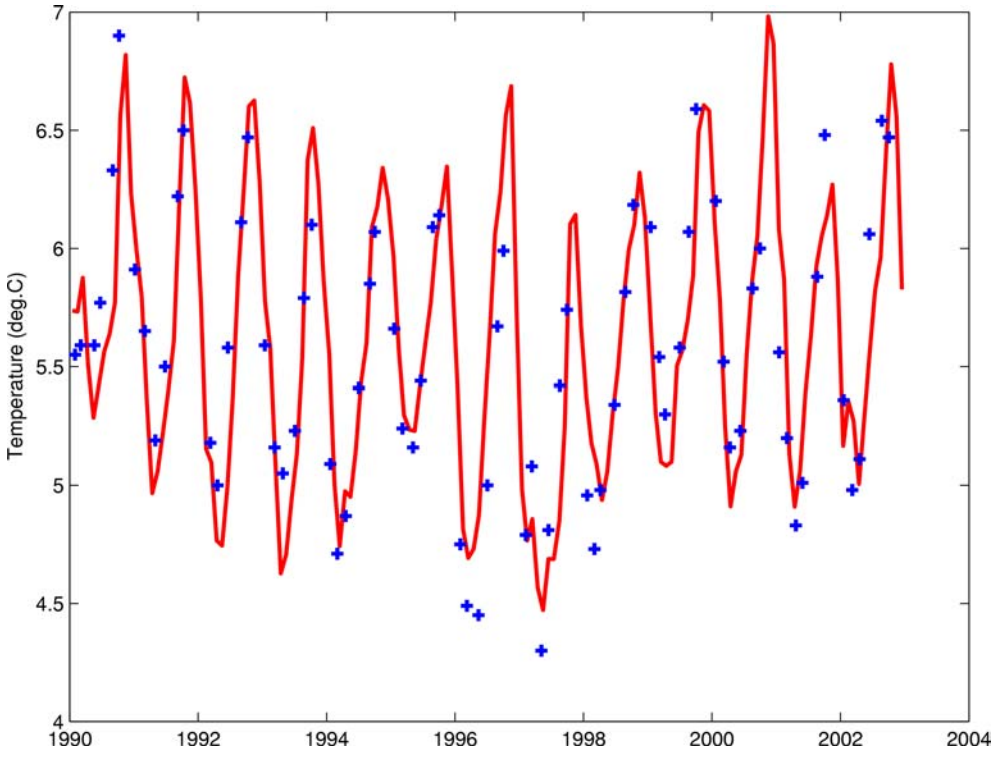

Fig. 9 Modelled monthly mean (*red*) and observed (*blue*) time series of the mean Fugløya-Bjørnøya section temperatures. Averages are computed over a depth range of 50–200 m, and from 71.5–73.5°N

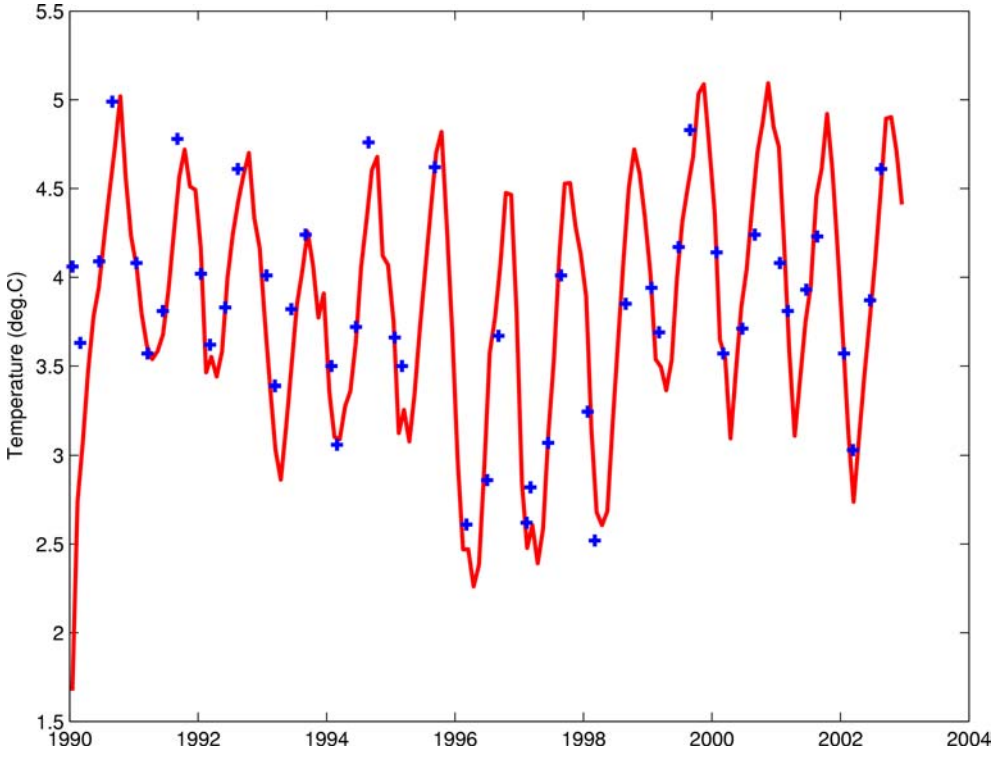

Fig. 10 Modelled monthly mean (*red*) and observed (*blue*) time series of the mean Vardø N section temperatures. Averages are computed over a depth range of 50–200 m, and from 72.25–74.25°. Note that the model values shown have been reduced by a constant 0.5°C

The overall error statistics are provided in Table 1. There is negligible bias in the modelled Fugløya-Bjørnøya results, but the bias in the Vardø North and Kola results are appreciable. The higher bias at the Kola section than at Vardø North is attributable to the 0–200 m depth range at Kola relative to the 50–200 m range at Vardø North used in constructing the averages. While the root-mean-square of the error after removal of

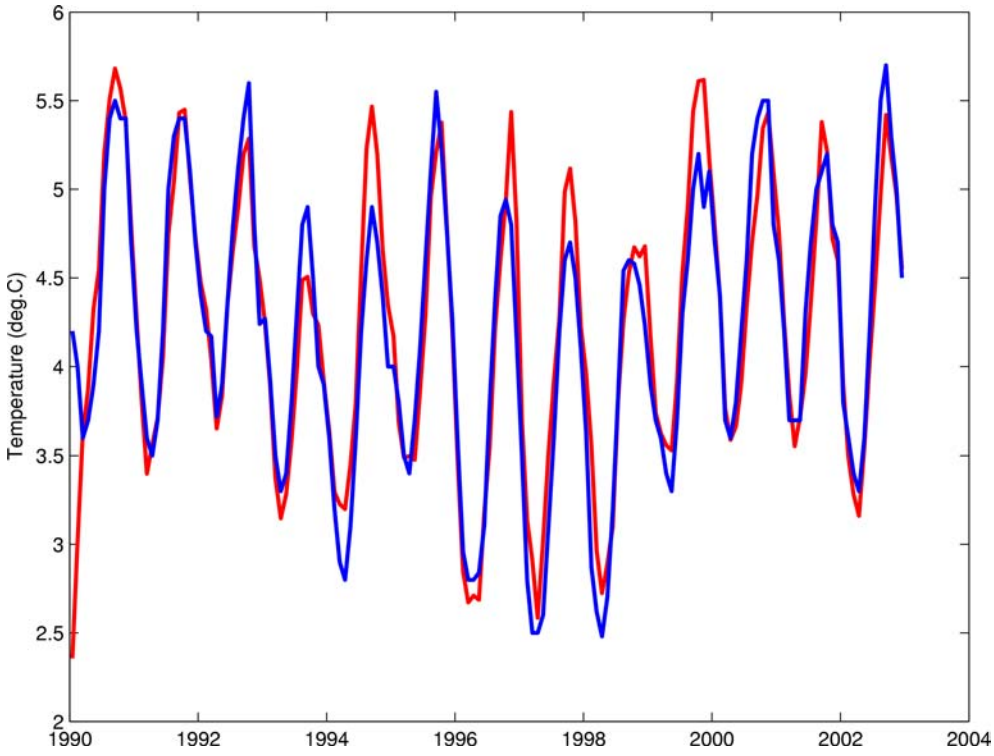

Fig. 11 Modelled (*red*) and observed (*blue*) monthly mean time series of the mean Kola section temperatures. Averages are computed over a depth range of 50–200 m, and from 70.5–72.5°N Note that the model values shown have been reduced by a constant 0.6°C

Table 1 Mean error (bias) and root-mean-square error with the bias removed for the Fugløya-Bjørnøya, Vardø North and Kola section mean temperatures based on the period 1991–2002

Section	Mean error (°C)	$RMSE_u$ (°C) bias removed
Fugløya-Bjørnøya	0.00	0.26
Vardø North	0.48	0.23
Kola	0.63	0.26

the bias (denoted $RMSE_u$) is comparable in the three sections, the bias error at the Vardø North and Kola sections is over twice the $RMSE_u$ and accounts for over 80% of the total mean-square error. As will be shown later, the cause of this positive bias error is likely the excessive inflow of Atlantic Water in the model results.

3.1.3 Barents inflow

The inflow of warmer Atlantic Water through the western entrance of the Barents Sea plays an important role in determining the temperature and ice distribution in the Barents (Ådlandsvik and Loeng 1991; Loeng et al. 1997). Shown in Fig. 12 is the net inflow volume flux across the Fugløya-Bjørnøya section. It can be seen that the seasonal variability is an order of magnitude higher than the inter-annual variability.

Over the period 1991–2002, the mean net volume flux of inflow to the Barents across the Fugløya-Bjørnøya section is computed to be 3.2 Sv ($1\ Sv = 10^6\ m^3\ s^{-1}$). Across the full Barents entrance between northern Norway and the southern tip of Spitzbergen, the net inflow over the period 1991–2002 is computed to be 3.6 Sv in this study. Maslowski et al. (2004) computed a value of 3.3 Sv net inflow across the same section in their study. From fixed current meter mooring arrays, Ingvaldsen et al. (2004b) estimated net Atlantic Water inflow to the Barents through the Fugløya-Bjørnøya section to be 1.5 Sv, averaged over the period August 1, 1997 through July 31, 2001. If Atlantic Water is taken to be water warmer than 3°C with salinity greater than 34.9, then on the same section, over the same period, a value of 2.5 Sv is obtained in this modelling study. The advective heat flux computed from current meter mooring temperature and currents for the same period is 35.4 TW, whereas the heat flux computed from model results using the same 'sampling' scheme as the observations is 80.4 TW.

Since the modelled temperatures at the Barents Opening (Fugløya-Bjørnøya) are unbiased, the excessive modelled heat flux must be due to too high inflow velocities. It is possible that the NCEP/NCAR Reanalysis daily mean wind stresses are too high. Renfrew et al. (2002) have noted that the roughness length formula employed in the computation of surface momentum flux in the NCEP reanalysis project is inappropriate for moderate to high wind speeds and that errors can be substantial in regions with large air–sea temperature differences and high wind speeds (such as the western Barents Sea and the Norwegian Sea). Such a formulation could produce an over-estimate of wind stress during storm events, precisely the conditions favourable

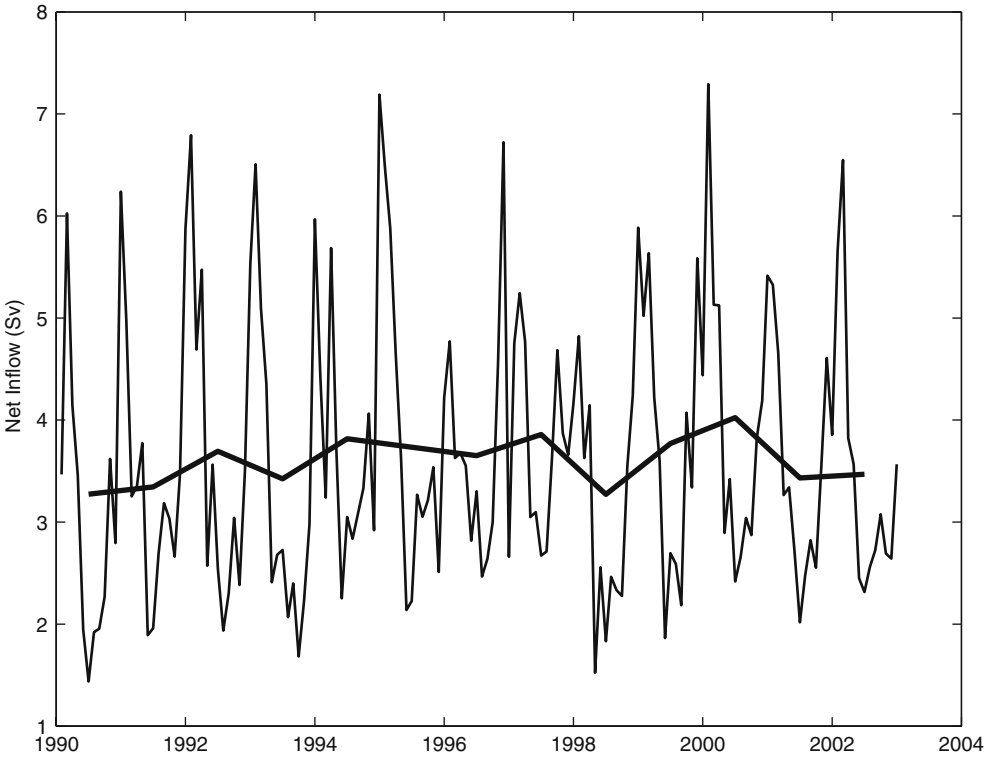

Fig. 12 Monthly (*thin line*) and annual (*thick line*) mean time series of the computed net inflow across the Fugløya-Bjørnøya section. The seasonal variability of the volume transport is an order of magnitude larger than the inter-annual variability

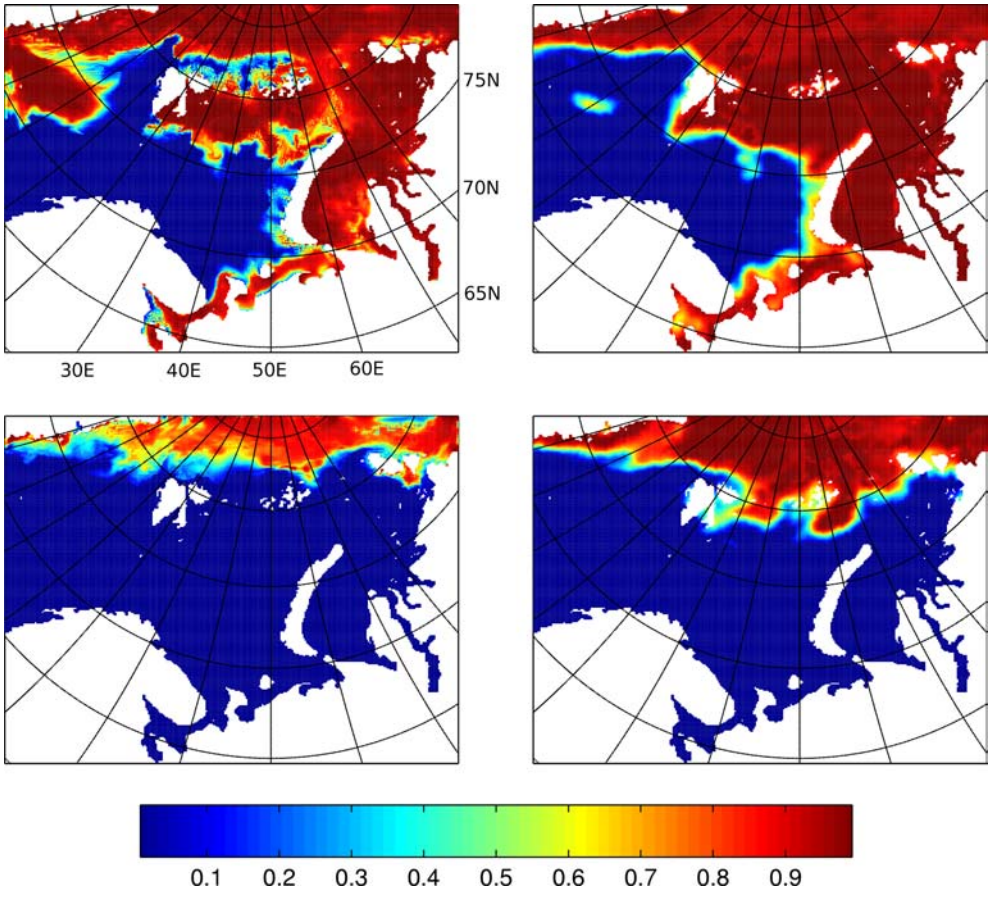

Fig. 13 Modelled versus Special Sensor Microwave/ Imager (SSM/I) daily mean ice concentrations. The *top row* is from March 20, 1993, the *lower row* is from September 20, 1993. The *left-hand column* contains the model fields, the *right-hand panel* contains the SSM/I fields. The March modelled ice edge locations in the northern and southern Barents are in good agreement with observations, but show too much ice in the Greenland Sea and too little north and east of Spitzbergen. The September model results show an ice edge displaced to the north of the observed ice edge

to Barents inflow (R. Ingvaldsen, personal communication). This hypothesis is currently being tested through sensitivity analyses with a variety of atmospheric forcing fields.

3.1.4 Satellite ice concentration

Sea ice concentration in the Barents Sea can exhibit considerable variation both seasonally and inter-annually (Gloersen et al. 1992). Typical ice concentration distributions from the maximum and minimum ice extent periods during the year are shown in Fig. 13. Given that the fields shown are daily mean values and, thus, effectively snap shots of ice distributions, the agreement between model fields and observations is remarkably good. The SSM/I (Special Sensor Microwave/Imager) data has a spatial resolution of 25 km, whereas the model resolution is ~9 km. The satellite values are linearly interpolated on to the model grid and will appear somewhat smoother than the modelled values. The locations of the March modelled ice edges in the northern Barents (76°N) and in the south-eastern Barents (69°N) are in good agreement with observations. The model results show too much ice in the Greenland Sea and too little ice north of Spitzbergen along 82–85°N, between 20–50°E. The September model results are in good general agreement with the observations, but show too much ice-melt. The modelled ice edge is too far to the north.

To obtain an integral estimate of model performance, the monthly mean total areal ice cover has been tabulated from model results and from SSM/I satellite data. Figure 14 shows that the model results successfully track the seasonal and inter-annual variability, but that there is a systematic under-estimation of summer ice cover, consistent with the September results shown in Fig. 13. The modelled under-estimate of ice concentration in summer is likely attributable to excessive shortwave radiation.

It was argued previously that the positive bias in modelled temperatures 'downstream' of the Barents Opening is likely due to excessive inflow of Atlantic Water. If that is the case, one should expect to see a negative bias in the ice cover in the central Barents Sea. This condition is confirmed in Fig. 15. The model results show a nearly constant offset of -1×10^5 km^2 from the observations in the 12-month running mean. While there is a clear bias in the annual mean, the model results closely match the observed inter-annual fluctuations and perturbations.

4 Ice–ocean interaction

Ice freezing and melting processes have the potential to modify water mass characteristics through brine rejection and subsequent intermediate and deep water formation during the freezing process and through freshening of surface layers during the melting process. The total ice formation in meters of ice produced during the year 1993 as estimated from the model results is shown in Fig. 16. The ice production is highest along

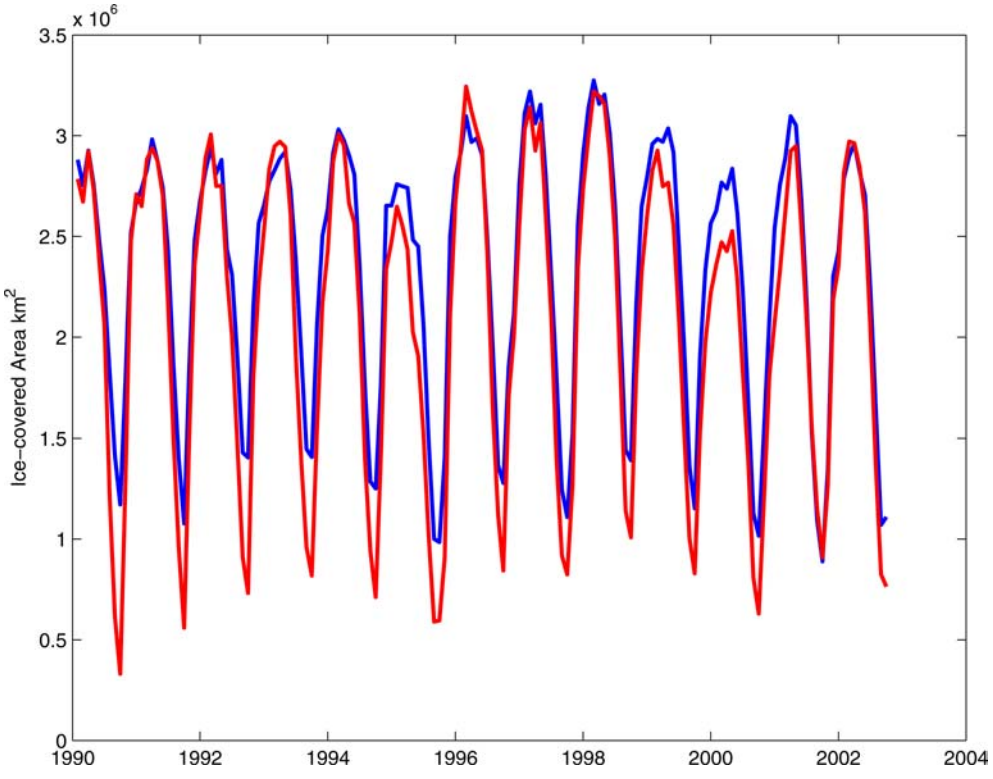

Fig. 14 Monthly mean modelled (*red*) and SSM/I (*blue*) time series of the ice-covered area in the model domain

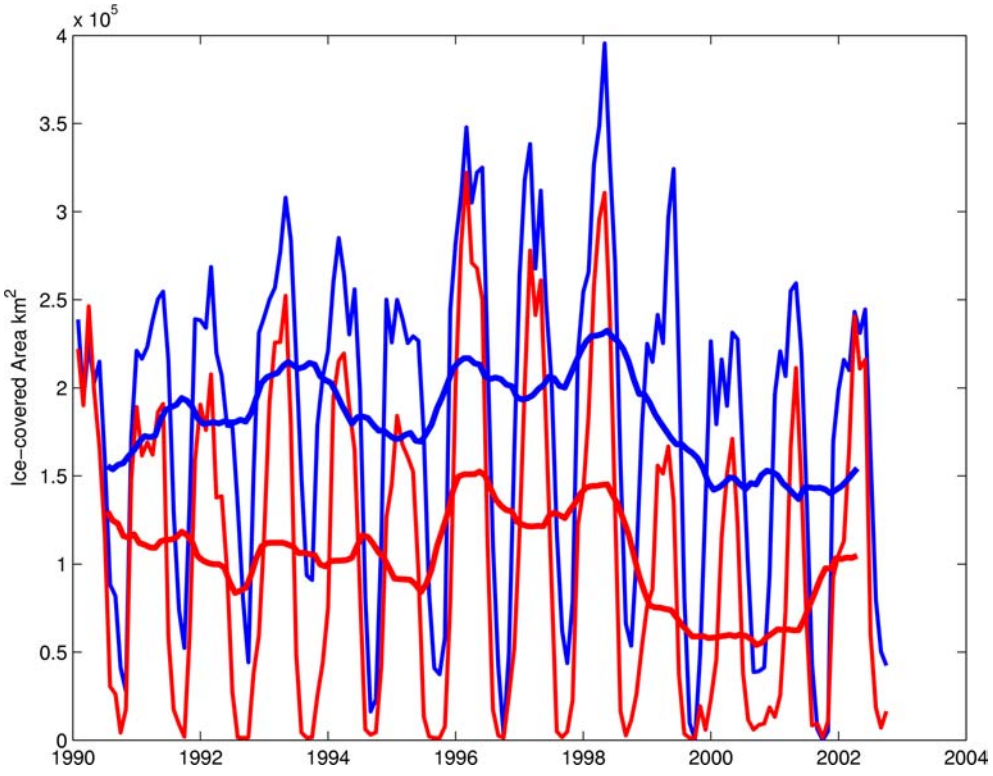

Fig. 15 Monthly mean modelled (*red*) and SSM/I (*blue*) time series of the ice-covered area in the region from 71°N to 82°N and 25°E to 45°E. The thicker lines are 12-month running means of the monthly values

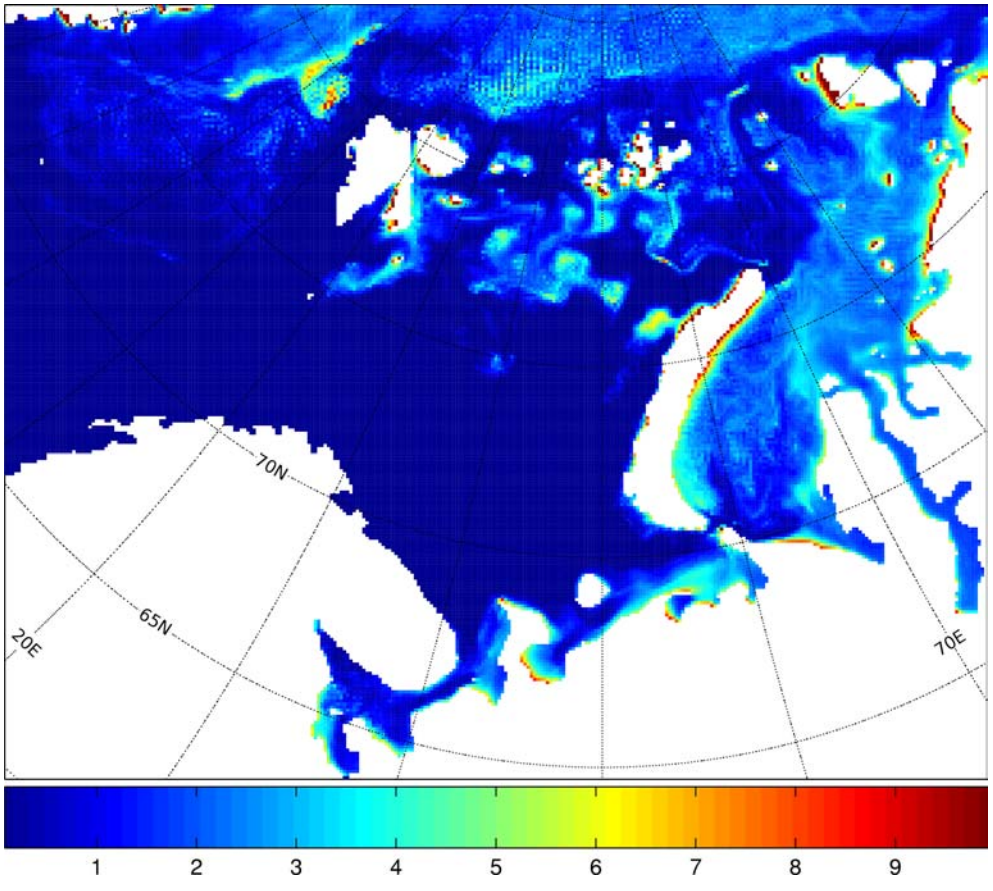

Fig. 16 Distribution of total ice production (m) for the year 1993 as estimated from the model results. The most efficient ice-production areas are over banks and in shallow near-shore zones

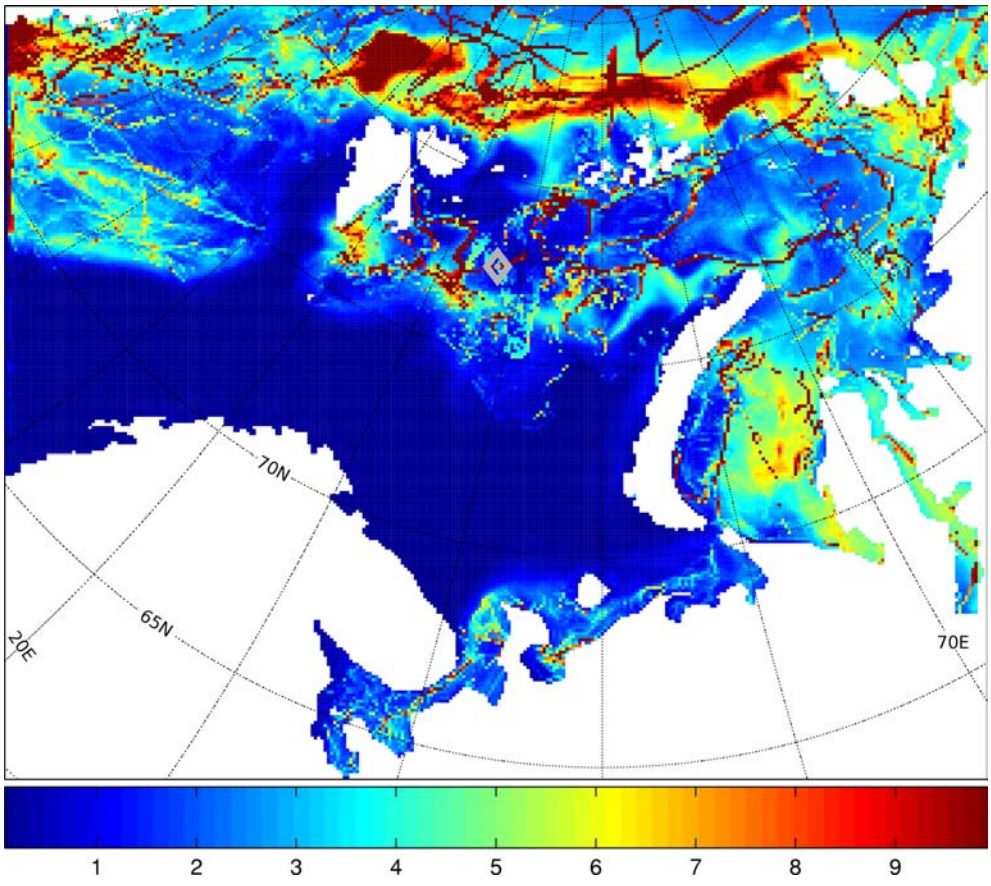

Fig. 17 Distribution of total ice melt (m) for the year 1993 as estimated from the model results. The *grey diamond* marks the location of the ice-melt time series of Fig. 18. Most ice-melt takes place along the northern Barents ice-edge in summer and along narrow lines in rapid melting events

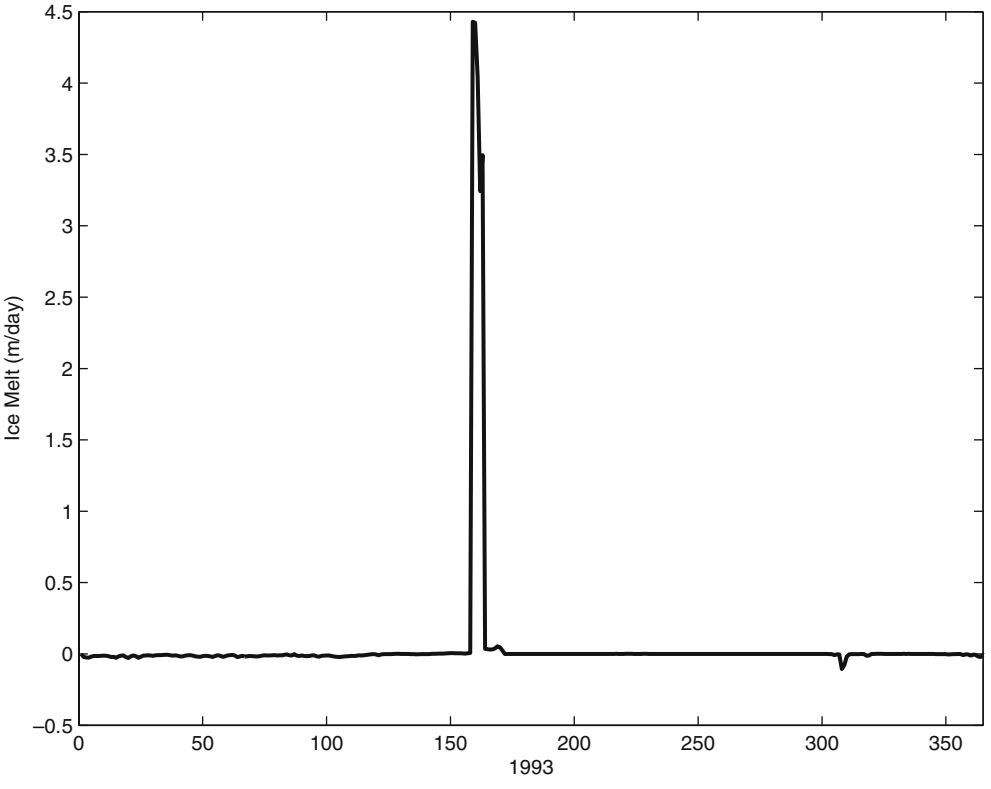

Fig. 18 Daily mean time series of ice-melt rates (m/day) for 1993 at the location marked in Fig. 17

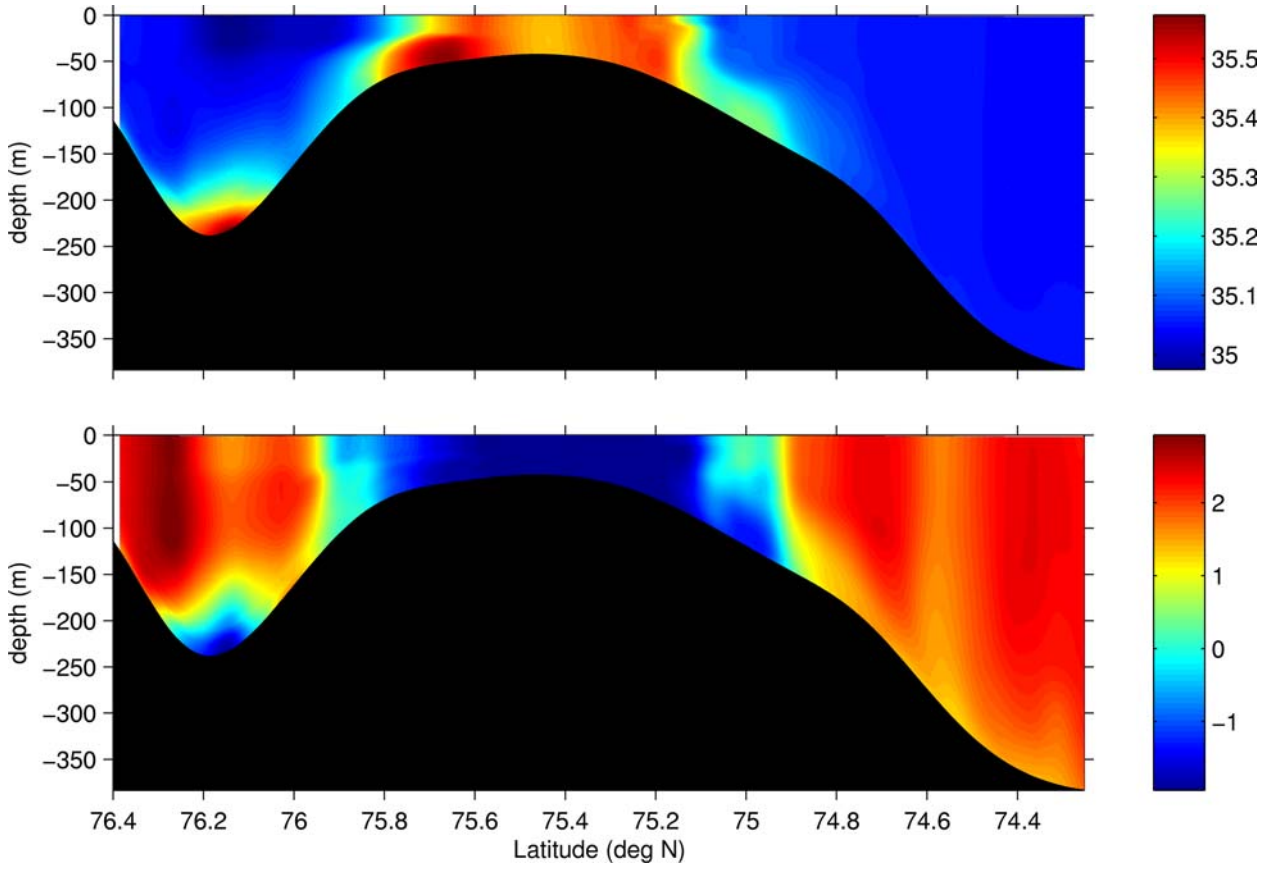

Fig. 19 Daily mean simulated salinity (*top panel*) and temperature (*bottom panel*) for March 31, 1993 at the Spitzbergen Bank section (section S in Fig. 1). Ice formation produces high-salinity brines over the shallow bank. The brines drain down both sides of the bank, the brines from the north slope accumulate in Storfjord Trough

coastal polynyas in the Kara Sea and polynyas situated around the islands of the northern Barents. Broad areas of ice production exist in the Kara Sea, over the banks of the northern half of the Barents Sea and in the White and Pechora Seas along the south coast of the model domain.

The distribution of total ice-melt for 1993, shown in Fig. 17, is very different from that of ice formation. While most ice-melting occurs in a region encompassing the summer ice edge in the northern Barents, discontinuous lines of high total ice-melt are distributed throughout the portion of the model domain which encounters ice cover. A sample time series of ice-melt rates at one location situation on a high ice-melt line is shown in Fig. 18. The melting is concentrated in a 5–8 day period in early June, with no other appreciable melt activity occurring over the rest of the year. The rapid melting event corresponds to the transport of the ice edge into surface waters previously warmed by shortwave radiation. The melting occurs largely through lateral ablation.

As can be seen from Fig. 16, the Spitzbergen Bank (section S in Fig. 1) is a zone of significant ice production. When ice forms, brines are ejected. These brines enhance the surface salinity and increase the density of the surface water which then sinks to form a dense, saline layer at the bottom. The drainage of brine-enriched waters down the slopes of the Spitzbergen Bank is shown in Fig. 19. Plumes of brine-enhanced salinity can be seen draining down both sides of the bank. The plume on the north (left) side of the bank forms a thin bottom layer in the Storfjord Trough. The brine drainage on the south (right) side of the bank is more diffuse, due to the stronger tidal mixing on the south side. Over the shallowest portion of the bank, the water column is vertically homogeneous, with the temperature at the freezing point. The warm core over the northern portion of the Storfjord Trough (far left of figure) is due to an intrusion from the West Spitzbergen Current.

Another high ice-production region is situated west of Novaya Zemlya along section N in Fig. 1. Shown in Fig. 20 are the simulated daily mean temperature and salinity from that section for February 28, 1994. A column of brine-enriched water is situated over the shallowest portion of the bank. Other, weaker brine-enhanced columns exist in deeper waters in the western (left-hand) portion of the section. The weaker columns in deeper water are attributable to the hydrostatic property of ROMS: convection is represented as a vertical mixing process. Thus, there is likely to be more

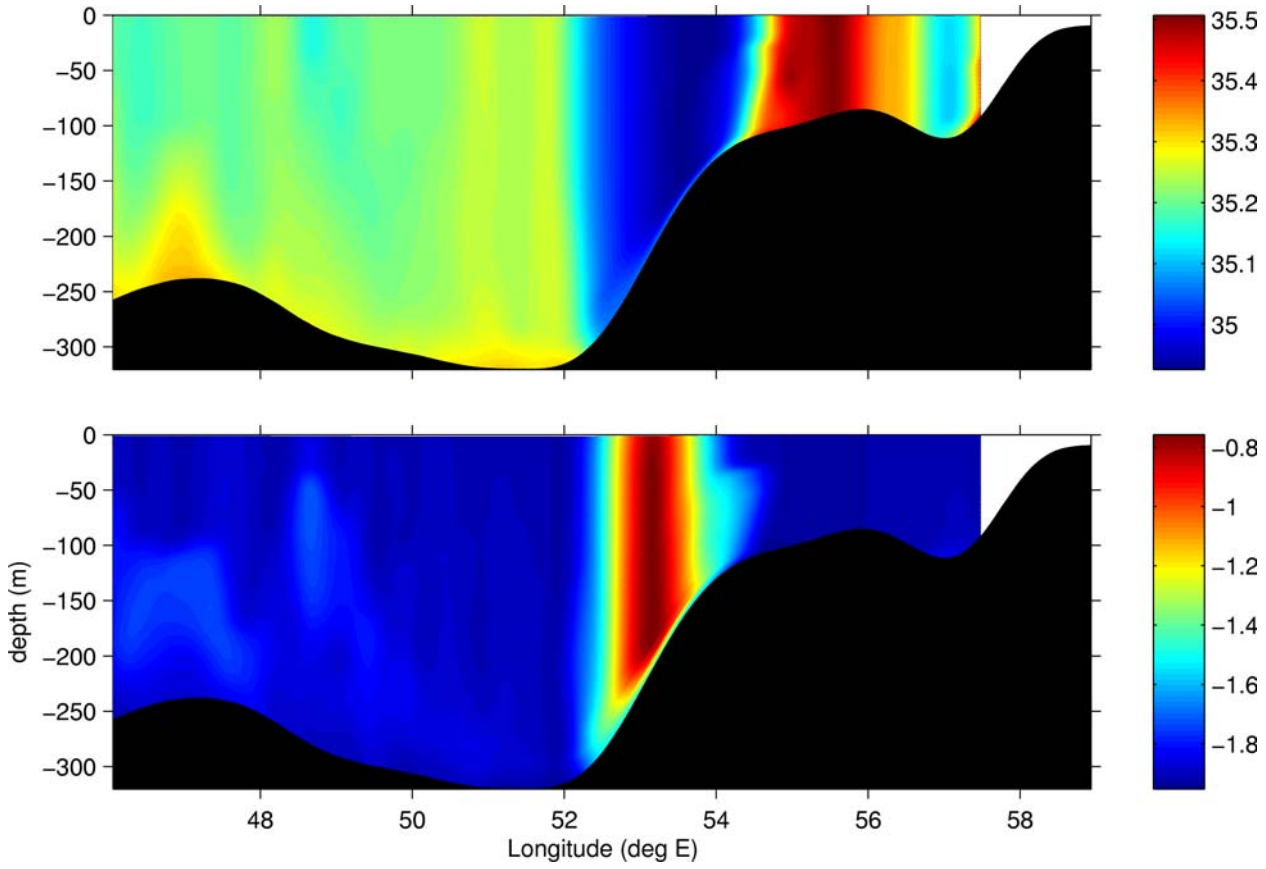

Fig. 20 Daily mean simulated salinity (*top panel*) and temperature (*bottom panel*) for February 28, 1994 at the West Novaya Zemlya section (section N in Fig. 1). Intense brine formation occurs over the bank at 54–56°E. Along the bank slope (53°E is the last vestige of the Atlantic Water inflow in a northward-flowing jet

dilution of brines within ROMS in deeper waters than occurs in nature where brines can sink to the bottom with much less entrainment of surrounding water masses. Along the western slope of the main bank at the

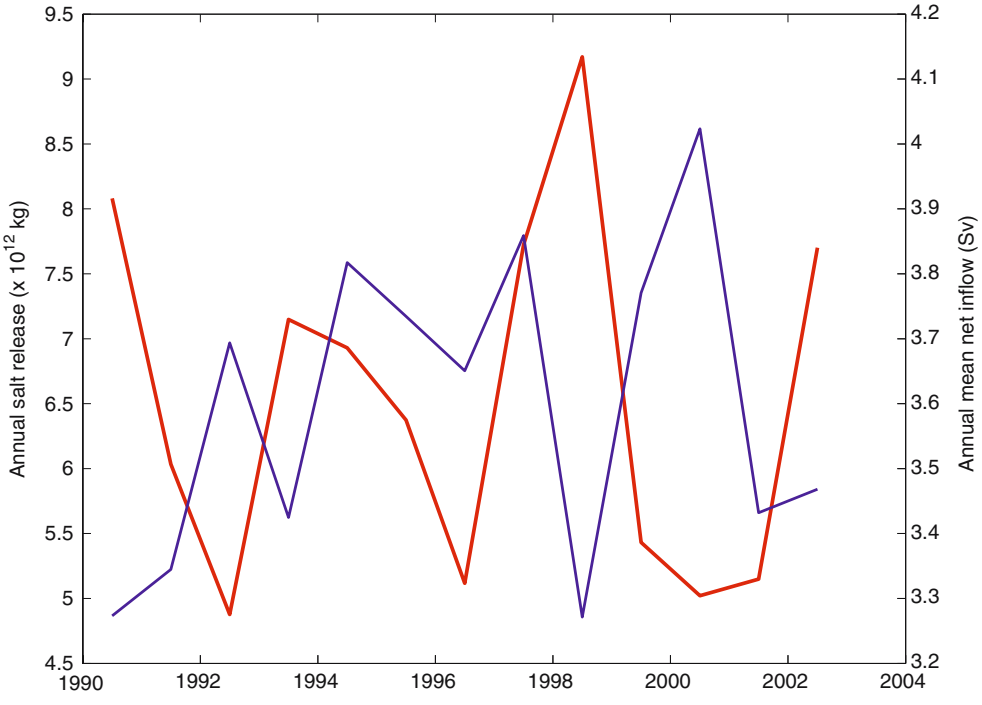

Fig. 21 Salt release (*red*) and net volume inflow across the Fugløya-Bjørnøya section (*blue*) time series. Salt release is computed for the region between 71 and 82°N and 25–45°E in the Barents Sea

centre of the section the last vestige of Atlantic Water inflow appears as the warmer, less saline core of a northward-flowing along-slope jet.

An integrated annual estimate of salt production from brine rejection in the freezing process provides a good indication of the year-to-year variation in water mass formation and modification. Dramatic variations in salt production in the north-central Barents can be seen in the time series of Fig. 21. With the exception of 1996, there is a clear correspondence between years of high salt release and low Barents inflow. This is consistent with lower ice production during years of higher inflow of warmer Atlantic Water.

5 Concluding remarks

The main goals of this study are to assess model performance in the light of available observations and determine the model's utility for dynamical downscaling applications. The agreement between simulated and observed temperatures is, in general, excellent. The notable exceptions are the bias in simulated temperatures at the Vardø North and Kola sections. The likely cause of this bias error is excessive inflow of warm Atlantic Water at the Barents western entrance.

The agreement between modelled and observed salinities is not as close as with temperature, particularly at the Fugløya-Bjørnøya section. There, the model produces a weaker, more saline coastal current. This error is largely attributable to the relatively low salinity Norwegian Coastal Current not being adequately spatially resolved at the southern open boundary with forcing from the 50 km resolution Large Area model. The more saline, less stratified model results near Bjørnøya may be caused by the simulated ice edge lying a few kilometres too far to the north.

The agreement between total simulated and observed sea ice cover during 10 months of the year is excellent. During summer, however, the model results show excessive melting of sea ice occurring in the northern Barents. While it was found that, as noted by Serreze et al. (1998), NCEP/NCAR Reanalysis cloud fraction is too low and that ISCCP cloud cover data is more realistic at high latitudes, it is clear from the Makshtas and Korsnes (2001) study that the ISCCP cloud fraction in the northern Barents marginal ice zone in summer is still too low. An improved parameterization for the effect of low cloud/fog over the Barents summer marginal ice zone on the radiation budget is required if the summer ice melting is to be reduced. The model results underestimate the ice cover in the central Barents region with a nearly constant offset. The negative bias is consistent with too much inflow of Atlantic Water into the Barents. The modelled ice cover in the central Barents does, however, closely follow the observed inter-annual fluctuations.

The computed net inflow volume flux across the Barents Opening is within 10% of that of the Maslowski et al. (2004) study, in which very different forcing fields were used. However, the computed Atlantic Water net inflow in this study is 1.67 times that estimated by Ingvaldsen et al. (2004b) from current meter moorings. This discrepancy could be largely attributable to uncertainty in the wind forcing fields in the western Barents/eastern Norwegian Sea. The sensitivity of the modelled Barents inflow to different forcing data sets is being examined in a study currently being conducted.

The coupled model can be used to examine the role of ice freezing and melting processes in water mass formation and modification. The spatial distribution of ice freezing and melting zones is quite different with freezing taking place largely over banks and in shallow regions and melting occurring in the summer marginal ice zone and at the ice edge. Lateral ablation at the ice edge is very episodic over 5–8 day period and along discontinuous lines. Brines released during the freezing process are found to drain from the banks in plumes, forming a brine-enhanced high-salinity layer in troughs and depressions. The salt released during freezing exhibits considerable inter-annual variability and tends to follow the opposite trend to the net inflow volume flux at the Barents western entrance.

Overall, the coupled model produces realistic seasonal and inter-annual ice-ocean variability. The discrepancies with observations can largely be accounted for by uncertainties in the prescribed forcing fields. Thus, the model is demonstrated to be a viable tool for ocean climate dynamical downscaling purposes.

Acknowledgements This work was supported by the Research Council of Norway Regional Climate development under global warming (RegClim) programme. This work has received support through the Programme for Supercomputing of the Research Council of Norway through a grant of computing time. I wish to thank Randi Ingvaldsen for making available her processed hydrographic section data and sharing her insight into circulation processes in the western Barents. I also wish to thank Jens Debernard and Øyvind Sætra for making available their EVP ice dynamics code and to Sirpa Häkkinen for making available her ice thermodynamics code.

References

Ådlandsvik B, Hansen R (1998) Numerical simulation of the circulation in the Svalbardbanken area in the Barents Sea. Cont Shelf Res 18:341–355

Ådlandsvik B, Loeng H (1991) A study of the climate system in the Barents Sea. Polar Res 10(1):45–49

Asplin L, Ingvaldsen R, Loeng H, Ådlandsvik B (1998) Description and validation of a 3-dimensional numerical model of the Nordic and Barents Seas. Fisken og Havet Rep 10. Inst of Mar Res, Bergen, Norway

Bentsen M, Drange H (2000) Parameterizing surface fluxes in ocean models using the NCEP/NCAR reanalysis data. In: RegClim General Technical Report No 4, Norwegian Institute for Air Research, Kjeller, Norway, pp 44–57

Bentsen M, Evensen G, Jenkins AD, (1999) Coordinate transformation on a sphere using conformal mapping. Mon Wea Rev 127:2733–2740

Chapman DC (1985) Numerical treatment of cross-shelf open boundaries in a barotropic coastal ocean model. J Phys Oceanogr 15:1060–1075

Dippner JW, Ottersen G (2001) Cod and climate variability in the Barents Sea. Clim Res 17(1):73–82

Ellertsen B, Fossum P, Solemdal P, Sundby S (1989) Relations between temperature and survival of eggs and first feeding larvae of the North-East Arctic cod (*Gadus morhua L.*). Rapports et Procs-verbaux des Runions du Conseil international pour lExploration de la Mer 191:209–219

Engedahl H (1995) Use of the flow relaxation scheme in a three-dimensional baroclinic ocean model with realistic topography. Tellus 47A:365–382

Flather RA (1976) A tidal model of the northwest European continental shelf. Mem Soc Roy Sci Liege Ser 6(10):141–164

Furevik T, Bentsen M, Drange H, Kindem IKT, Kvamstø NG, Sorteberg A (2003) Description and evaluation of the Bergen Climate Model: ARPEGE coupled with MICOM. Clim Dyn 21:27–51

Gloersen P, Campbell WJ, Cavalieri DJ, Comiso JC, Parkinson CL, Zwally HJ (1992) Arctic and Antarctic Sea Ice, 1978–1987: satellite passive-microwave observation and analysis. NASA Scientific and Technical Information Program, National Aeronautics and Space Administration, Washington, DC

Haidvogel DB, Beckmann A (1999) Numerical ocean circulation modeling. Imperial College Press, London

Haidvogel DB, Arango HG, Hedström K, Beckmann A, Malanotte-Rizzoli P, Shchepetkin AF (2000) Model evaluation experiments in the North Atlantic Basin: simulations in nonlinear terrain-following coordinates. Dyn Atmos Ocean 32:239–281

Häkkinen S, Mellor GL (1992) Modelling the seasonal variability of a coupled arctic ice-ocean system. J Geophys Res 97:20285–20304

Harms IH (1992) A numerical model of the barotropic circulation in the Barents and Kara Seas. Cont Shelf Res 12(9):1043–1058

Harms IH (1997) Water mass transformation in the Barents Sea—application of the Hamburg shelf ocean model (HamSOM). ICES J Mar Sci 54(3):351–365

Hunke E (2001) Viscous-plastic sea ice dynamics with the EVP model: linearization issues. J Comput Phys 170:18–38

Hunke E, Dukowicz J (1997) An elastic-viscous-plastic model for sea ice dynamics. J Phys Oceangr 27:1849–1867

Ingvaldsen R, Asplin L, Loeng H (2004a) Velocity field of the western entrance to the Barents Sea. J Geophys Res 109(C030201). DOI 10.1029/2003JC001811

Ingvaldsen R, Asplin L, Loeng H (2004b) The seasonal cycle in the Atlantic transport to the Barents Sea during the years 1997–2001. Cont Shelf Res 24:1015–1032

Kalnay E, Kanamitsu M, Kistler R, Collins W, Deaven D, Gandin L, Iredell M, Saha S, White G, Woollen J, Zhu Y, Chelliah M, Ebisuzaki W, Higgins W, Janowiak J, Mo KC, Ropelewski C, Wang J, Leetma A, Reynolds R, Jenne R, Joseph D (1996) The NCEP/NCAR 40-year reanalysis project. Bull Am Met Soc 77(3):437–471

Large WG, Gent PR (1999) Validation of vertical mixing in an equatorial ocean model using large eddy simulations with observations. J Phys Oceangr 29:449–464

Large WG, McWilliams JC, Doney SC (1994) Oceanic vertical mixing: a review and a model with a nonlocal boundary layer parameterization. Rev Geophys 32:10937–10954

Loeng H, Ozhigin V, Ådlandsvik B (1997) Water fluxes through the Barents Sea. ICES J Mar Sci 54(3):310–317

Makshtas AP, Korsnes R (2001) Distribution of solar radiation in the Barents Sea marginal ice zone during summer. J Geophys Res 106(C2):2531–2543

Maslowski W, Marble D, Walczowski W, Schauer U, Clement JL, Semtner AJ (2004) On climatological mass, heat, and salt transports through the Barents Sea and Fram Strait from a pan-Arctic coupled ice-ocean model simulation. J Geophys Res 109(C03032). DOI 10.1029/2001JC001039

Mellor GL, Kantha L (1989) An ice-ocean coupled model. J Geophys Res 94:10937–10954

Mellor GL, Yamada T (1982) Development of a turbulence closure-model for geophysical fluid problems. Rev Geophys 20(4):851–875

Mellor GL, McPhee MG, Steele M (1986) Ice seawater turbulent boundary–layer interaction with melting or freezing. J Phys Oceanogr 16(11):1829–1846

Michalsen K, Ottersen G, Nakken O (1998) Growth of North-east Arctic cod (Gadus morhua L.) in relation to ambient temperature. ICES J Mar Sci 55:863–877

Nakken O, Raknes A (1987) The distribution and growth of Northeast Arctic cod in relation to bottom temperatures in the Barents Sea, 1978–1984. Fish Res 5:243–252

Oki T, Sud YC (1998) Design of Total Runoff Integrating Pathways (TRIP): a global river channel network. Earth Interactions 2. http://EarthInteractions.org

Padman L, Erofeeva S (2004) A barotropic inverse tidal model for the Arctic Ocean. Geophys Res Lett. DOI 10.1029/2003GL019003

Renfrew IA, Moore GWK, Guest PS, Bumke K (2002) A comparison of surface layer and surface turbulent flux observations over the Labrador Sea with ECMWF analyses and NCEP reanalyses. J Phys Oceangr 32:383–400

Sætersdal G, Loeng H (1987) Ecological adaptation of reproduction in Northeast Arctic cod. Fish Res 5:253–270

Sakshaug E, Bjorge A, Gulliksen B, Loeng H, Mehlum F (1994) Structure, biomass distribution, and energetics of the pelagic ecosystem in the Barents Sea—a synopsis. Polar Biol 14(6):405–411

Schiffer RA, Rossow WB (1985) ISCCP global radiance data set—a new resource for climate research. Bull Am Met Soc 66(12):1498–1505

Serreze MC, Key JR, Box JE, Maslanik JA, Steffen K (1998) A new monthly climatology of global radiation for the Arctic and comparisons with NCEP-NCAR reanalysis and ISCCP-C2 fields

Shchepetkin AF, McWilliams JC (2003) A method for computing horizontal pressure-gradient force in an oceanic model with a nonaligned vertical coordinate. J Geophys Res 108(C3). DOI 10.1029/2001JC001047

Song Y, Haidvogel D (1994) A semi-implicit ocean circulation model using a generalized topography-following coordinate system. J Comput Phys 115:228–244

Steele M, Morley R, Ermold W (2001) A global ocean hydrography with a high quality Arctic Ocean. J Clim 14:2079–2087

Stolehansen K, Slagstad D (1991) Simulation of currents, ice melting and vertical mixing in the Barents Sea using a 3-d baroclinic model. Polar Res 10(1):33–44

Warner JC, Geyer WR (2005) Numerical modelling of an estuary: a comprehensive skill assessment. J Geophys Res 110:C05001. DOI 10.1029/2004JC002691

Warner JC, Sherwood CR, Arango HG, Signell RP (2005) Performance of four turbulence closure methods implemented using a generic length scale method. Ocean Model 8:81–113